Research Square

Preprints are preliminary reports that have not undergone peer review.
They should not be considered conclusive, used to inform clinical practice,
or referenced by the media as validated information.

Research on the node placement strategies of absolute node coordinate formulation based on collocation method

Jia Wang

wangjia@sut.edu.cn

Shenyang University of Technology

Hao Zhang

Shenyang University of Technology

Lipeng Zhang

Beijing Institute of Aerospace Long March Flight Vehicles

Tengfei Wang

State Key Laboratory of Mechanical Structure Strength and Vibration

Research Article

Keywords:

Posted Date: November 23rd, 2026

DOI: https://doi.org/10.21203/rs.3.rs-11593228/v1

License: This work is licensed under a Creative Commons Attribution 4.0 International License.
Read Full License

Additional Declarations: No competing interests reported.

Research on the node placement strategies of absolute node coordinate formulation based on collocation method

Jia Wang, Hao Zhang, Lipeng Zhang, Tengfei Wang

Abstract

The convergence behavior and computational efficiency of beam elements based on the absolute nodal coordinate formulation (ANCF) are strongly influenced by the distribution of interpolation nodes and the choice of numerical quadrature. For high-order beam elements employing Hermite interpolation, a one-to-one correspondence between interpolation nodes and quadrature points may lead to insufficient integration accuracy, particularly when evaluating geometrically nonlinear elastic forces. To address this limitation, this study proposes a quadrature-consistent node configuration framework for ANCF-C beam elements, in which a subset of quadrature points is selected as position nodes while the complete points are retained for numerical integration. This approach allows the numbers of position nodes and quadrature points to be controlled independently while preserving their spatial consistency. Three node configuration strategies are investigated: uniformly distributed nodes combined with Newton–Cotes quadrature (S1), Legendre-based nodes combined with Legendre–Gauss–Lobatto quadrature (S2), and Chebyshev-based nodes combined with Clenshaw–Curtis quadrature (S3). Static bending benchmarks and dynamic flexible-pendulum simulations are conducted to evaluate the effects of these strategies on numerical accuracy, convergence behavior, and computational efficiency.

1 Introduction

Slender components, such as beams and cables in flexible multibody systems, often undergo large rotations together with substantial elastic deformation. Their numerical description must therefore account for geometric nonlinearity, the coupling between axial and bending deformations, and computational efficiency. The absolute nodal coordinate formulation (ANCF) uses global position vectors and their gradients as nodal variables and interpolates the configuration in an inertial reference frame, providing a unified kinematic description of these problems[1-2]. Within this framework, various elastic force models and three-dimensional beam, two-dimensional shear-deformable beam, thin-beam, and cable elements have been developed[3-8]. Subsequent studies have addressed appropriate representations of axial and bending strains and the construction of geometrically exact beam elements[9-10]. Reviews of ANCF developments and applications to multibody systems undergoing large deformations have also emphasized the importance of selecting suitable kinematic descriptions, strain models, and numerical implementations [11,23]

J. Wang(✉), H. Zhang
School of Mechanical Engineering, Shenyang University of Technology, NO.111, Shenliao West Road, Shenyang, China
E-mail: wangjia@sut.edu.cn

L. Zhang
Beijing Institute of Aerospace Long March Flight Vehicles

T. Wang
State Key Laboratory for Strength and Vibration of Mechanical Structures, School of Aerospace Engineering, Xi'an Jiaotong University, Xi'an 710049, Shaanxi, China

The computational performance of an ANCF beam element is closely related to its degrees of freedom, interpolation scheme, elastic force evaluation, and numerical quadrature. Garcia-Vallejo et al.[12] investigated efficient evaluation of the elastic forces and the Jacobian matrix. Zhang et al. [13]improved the computational efficiency of cable elements using a dot-product representation of curvature, while Taylor et al. [14,15]compared ANCF implementations and their effects on simulation performance. These studies indicate that both discretization accuracy and implementation cost must be considered when assessing element efficiency. For high-order polynomial discretization, the nodal distribution also affects the numerical stability of interpolation[17], whereas the quadrature rule and the number of quadrature points govern the approximation error in element-domain integrals[16,18]. Consequently, when internal position nodes are introduced to increase the discretization order, the effects of node placement and numerical quadrature should be examined separately.

In the development of multinode ANCF beam elements, Wang et al. [24,25]incorporated a node placement strategy based on Legendre polynomials and Lobatto quadrature and investigated element performance through static and dynamic examples. Their work provides a basis for examining the relationship between node placement and computational efficiency. In a related development, Ishaquddin and Gopalakrishnan[26] combined interior displacement degrees of freedom with boundary displacement and derivative degrees of freedom in weak-form quadrature elements for gradient elastic beams. Çevik et al.[27] reviewed the construction and application of polynomial bases and collocation methods. For multinode ANCF-C beams with endpoint gradient degrees of freedom, further investigation is needed to clarify the relationship between the collocation nodes and the complete set of quadrature points under unified kinematic and energy descriptions, and to compare the accuracy and cost of different nodal distributions and quadrature combinations.

This issue concerns the compatibility between interpolation constraints and quadrature sampling. In Hermite–Lagrange interpolation constructed from endpoint positions, endpoint gradients with respect to the axial material coordinate, and internal positions, the endpoint gradients provide additional independent interpolation conditions. Directly identifying every position node with a quadrature point may therefore leave the quadrature sampling insufficient to represent the full element interpolation space, introducing the risk of a rank-deficient mass matrix or underintegration of nonlinear elastic terms. These risks depend on the specific degrees of freedom and interpolation scheme and cannot be assessed solely from whether the nodes and quadrature points coincide. For the element considered here, quadrature resolution must be adjustable for a prescribed number of collocation degrees of freedom while preserving the spatial relationship between nodes and quadrature points.

To address this issue, a node selection method based on the complete set of quadrature points is proposed. A prescribed quadrature rule first generates the quadrature points, including the endpoints, and their weights. Position collocation nodes are then selected from this set subject to endpoint retention, left–right symmetry, and parity constraints on the number of nodes. When more than one admissible subset exists, the configuration is determined lexicographically using the 2-norm condition number of the scale-normalized Hermite interpolation matrix and a dimensionless basis-function amplification measure. Quadrature points not selected as collocation nodes, together with their weights, are retained in the evaluation of the mass, elastic, and gravity terms. Thus, the numbers of collocation nodes and quadrature points are no longer required to be equal, allowing spatial discretization and numerical quadrature to be coordinated within the same interpolation framework.

The present multinode beam formulation assigns axial gradient degrees of freedom to the endpoints and position degrees of freedom to all nodes. The elastic energy is constructed from the Green axial strain and geometric curvature, and differentiation of this energy yields the elastic internal force and stiffness matrix. Three combinations of node placement and quadrature are considered: equidistant nodes with closed Newton–Cotes quadrature (S1), Legendre–Gauss–Lobatto-type placement with Lobatto quadrature (S2), and Chebyshev–Gauss–Lobatto-type placement with Clenshaw–Curtis quadrature (S3). The study focuses on node subset

selection while retaining the complete quadrature set and on the numerical performance of the resulting configurations within the same kinematic, strain, and solution framework. Numerical examples are used to examinethe performance of the accuracy, efficiency, and the convergence. Two discretization procedures are considered: increasing the number of elements at a fixed number of nodes per element and increasing the number of nodes at a fixed number of elements. Section 2 presents the element model, Sect. 3 describes the placement strategies and node selection criteria, Sect. 4 discusses the numerical results, and Sect. 5 summarizes the main conclusions and their scope.

2 ANCF-C beam element formulation with node placement strategies

2.1 Element description

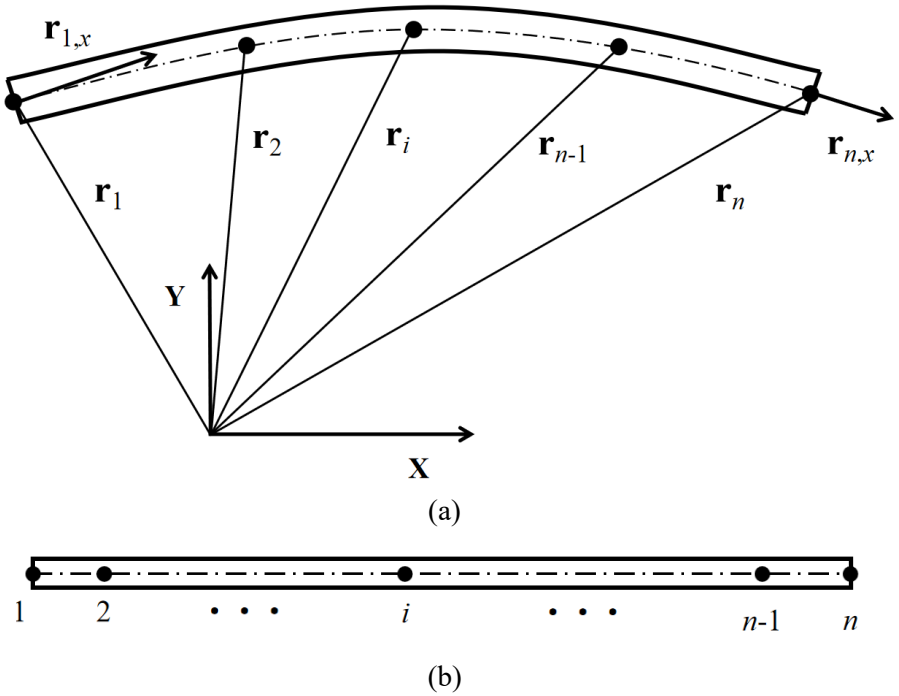


Fig1. Geometric description of a planar multi node ANCF-C beam element: (a) deformed configuration; (b) reference configuration

In case of multimode ANCF-C beam element, each element contains n nodes, as illustrated in Fig. 1. The position vectors and axial gradient vectors of the boundary node and, the position vectors of the internal nodes are chosen as the generalized coordinate of the element. The element generalized coordinate vector is expressed as

$$\mathbf{q}_e = \begin{bmatrix} \mathbf{r}_1^T & \mathbf{r}_{1,x}^T & \mathbf{r}_2^T & \cdots & \mathbf{r}_i^T & \cdots & \mathbf{r}_{n-1}^T & \mathbf{r}_n^T & \mathbf{r}_{n,x}^T \end{bmatrix}^T \tag{1}$$

where $\mathbf{r}_i$ is the position vector of node i. $\mathbf{r}_{1,x}$ and $\mathbf{r}_{n,x}$ are the axial gradient vectors of the boundary nodes. The position vector of an arbitrary point within the element is expressed as

$$\mathbf{r} = \mathbf{S}\mathbf{q}_e \tag{2}$$

where $\mathbf{S}$ is the shape functions of the element

$$\mathbf{S} = \begin{bmatrix} H_{10}\mathbf{I} & H_{11}\mathbf{I} & H_{20}\mathbf{I} & \cdots & H_{i0}\mathbf{I} & \cdots & H_{n0}\mathbf{I} & H_{n1}\mathbf{I} \end{bmatrix} \tag{3}$$

here, $H_1 \cdots H_n$ denotes the Hermite interpolation functions, and $\mathbf{I}$ is the third-order identity matrix. For an n-node element, the Hermite interpolation functions are given by

$$\begin{cases} H_{10}(\xi) = \dfrac{\xi-\xi_n}{\xi_1-\xi_n}\left\{1-(\xi-\xi_1)\left[L_{1,\xi}(\xi_1)+\dfrac{1}{\xi_1-\xi_n}\right]\right\}L_1(\xi) \\ H_{11}(\xi) = \dfrac{L_e}{2}\dfrac{(\xi-\xi_1)(\xi-\xi_n)}{\xi_1-\xi_n}L_1(\xi) \\ H_{i0}(\xi) = \dfrac{(\xi-\xi_1)(\xi-\xi_n)}{(\xi_i-\xi_1)(\xi_i-\xi_n)}L_i(\xi) \\ H_{n0}(\xi) = \dfrac{\xi-\xi_1}{\xi_n-\xi_1}\left\{1-(\xi-\xi_n)\left[L_{n,\xi}(\xi_n)+\dfrac{1}{\xi_n-\xi_1}\right]\right\}L_n(\xi) \\ H_{n1}(\xi) = \dfrac{L_e}{2}\dfrac{(\xi-\xi_1)(\xi-\xi_n)}{\xi_n-\xi_1}L_n(\xi) \end{cases} \tag{4}$$

where L_i and $L_{i,\xi}$ are the Lagrange interpolation functions and their first derivatives, respectively:

$$\begin{aligned} L_i(\xi) &= \prod_{\substack{j=1 \\ j\neq i}}^{n}\frac{\xi-\xi_j}{\xi_i-\xi_j}, \quad i=1,2,\ldots,n \\ L_{i,\xi}(\xi_i) &= \sum_{\substack{k=1 \\ k\neq i}}^{n}\frac{1}{\xi_i-\xi_k} \end{aligned} \tag{5}$$

Here, $\xi \in [-1,1]$ is the nondimensional coordinate of an arbitrary point within the element. The axial strain, geometric curvature, and endpoint gradients are defined using physical derivatives with respect to the material coordinate x. A coordinate transformation through the Jacobian J_e is therefore required. Denoting the element length by L_e, the relationship between the material and nondimensional coordinates is

$$x = \frac{L_e}{2}(1+\xi) \tag{6}$$

2.2 Stiffness matrix

The elastic strain energy of the element is

$$U_e = \frac{J_e}{2}\int_{-1}^{1} EA\varepsilon^2 + EI\kappa^2 d\xi \tag{7}$$

where ε is the axial strain, κ is the centerline curvature, E is Young's modulus, A is the cross-sectional area, and I is the second moment of area. The axial strain is defined from the Green strain tensor as

$$\varepsilon = \frac{1}{2}\left(\mathbf{r}_{,x}^{\mathrm{T}}\mathbf{r}_{,x} - 1\right) \tag{8}$$

$$\kappa = \frac{\left|\mathbf{r}_{,x} \times \mathbf{r}_{,xx}\right|}{\left|\mathbf{r}_{,x}\right|^3} \tag{9}$$

Here, $\mathbf{r}_{,x}$ and $\mathbf{r}_{,xx}$ are the first and second derivatives of the spatial position with respect to the material coordinate.

The elastic force is obtained by differentiating the elastic strain energy with respect to the generalized coordinates:

$$\mathbf{Q}_e = \frac{\partial U_e}{\partial \mathbf{q}_e} = J_e \int_{-1}^{1} \left(\mathbf{S}_{,x}^{\mathrm{T}} \mathbf{g}_u + \mathbf{S}_{,xx}^{\mathrm{T}} \mathbf{g}_v \right) \mathrm{d}\xi \tag{10}$$

where

$$\mathbf{g}_u = \left[\frac{EA}{2}(a-1) - \frac{2EIb}{a^3} + \frac{3EIc^2}{a^4} \right] \mathbf{u} - \frac{EIc}{a^3} \mathbf{v} \tag{11}$$

$$\mathbf{g}_{\mathrm{v}} = EI \left(\frac{\mathbf{v}}{a^2} - \frac{c}{a^3} \mathbf{u} \right) \tag{12}$$

with $\mathbf{u} = \mathbf{r}_{,x}$; $\mathbf{v} = \mathbf{r}_{,xx}$; $a = \mathbf{u}^T \mathbf{u}$; $b = \mathbf{v}^T \mathbf{v}$; and $c = \mathbf{u}^T \mathbf{v}$.

Differentiation of the elastic force with respect to the generalized coordinates gives the element stiffness matrix:

$$\mathbf{K}_e = \frac{\partial \mathbf{Q}_e}{\partial \mathbf{q}_e} = J_e \int_{-1}^{1} \begin{bmatrix} \mathbf{S}_{,x}^{\mathrm{T}} & \mathbf{S}_{,ss}^{\mathrm{T}} \end{bmatrix} \begin{bmatrix} \mathbf{H}_{uu} & \mathbf{H}_{uv} \\ \mathbf{H}_{uv}^{\mathrm{T}} & \mathbf{H}_{vv} \end{bmatrix} \begin{bmatrix} \mathbf{S}_{,x} \\ \mathbf{S}_{,xx} \end{bmatrix} \mathrm{d}\xi \tag{13}$$

where

$$\begin{aligned}
\mathbf{H}_{uu} &= \frac{EA}{2}(a-1) - \frac{2EIb}{a^3} + \frac{3EIc^2}{a^4}\mathbf{I} + \left[EA + \frac{12EIb}{a^4} - \frac{24EIc^2}{a^5} \right] \mathbf{u}\mathbf{u}^T \\
&+ \frac{6EIc}{a^4}(\mathbf{u}\mathbf{v}^T + \mathbf{v}\mathbf{u}^T) - \frac{EI}{a^3}\mathbf{v}\mathbf{v}^T \\
\mathbf{H}_{uv} &= -\frac{EIc}{a^3}\mathbf{I}_3 - \frac{4EI}{a^3}\mathbf{u}\mathbf{v}^T + \frac{6EIc}{a^4}\mathbf{u}\mathbf{u}^T - \frac{EI}{a^3}\mathbf{v}\mathbf{u}^T \\
\mathbf{H}_{vu} &= -\frac{EIc}{a^3}\mathbf{I}_3 - \frac{4EI}{a^3}\mathbf{v}\mathbf{u}^T + \frac{6EIc}{a^4}\mathbf{u}\mathbf{u}^T - \frac{EI}{a^3}\mathbf{u}\mathbf{v}^T \\
\mathbf{H}_{vv} &= \frac{EI}{a^2}\mathbf{I}_3 - \frac{EI}{a^3}\mathbf{u}\mathbf{u}^T
\end{aligned} \tag{14}$$

2.3 Mass matrix and equations of motion

The element kinetic energy is

$$T_e = \frac{1}{2}\int_0^{L_e} \rho A \dot{\mathbf{r}}^T \dot{\mathbf{r}}\, \mathrm{d}x = \frac{J_e}{2}\int_{-1}^{1} \rho A \dot{\mathbf{r}}^T \dot{\mathbf{r}} d\xi \tag{15}$$

where $\dot{\boldsymbol{r}}$ and $\ddot{\mathbf{r}}$ are the velocity and acceleration of an arbitrary point, respectively, and are expressed as

$$\begin{aligned} \dot{\mathbf{r}} &= \frac{\mathrm{d}\mathbf{r}}{\mathrm{d}t} = \mathbf{S}\dot{\mathbf{q}}_e \\ \ddot{\mathbf{r}} &= \frac{\mathrm{d}^2\mathbf{r}}{\mathrm{d}t^2} = \mathbf{S}\ddot{\mathbf{q}}_e \end{aligned} \tag{16}$$

Using $T_e == \frac{1}{2}\dot{\mathbf{q}}_e^T \mathbf{M}_e \dot{\mathbf{q}}_e$, the mass matrix is written as

$$\mathbf{M}_e = J_e \int_{-1}^{1} \rho A \mathbf{S}^{\mathrm{T}} \mathbf{S}\, \mathrm{d}\xi \tag{17}$$

The equations of motion are expressed as

$$\mathbf{M}\ddot{\mathbf{q}} + \mathbf{Q}_{\mathrm{int}}\left(\mathbf{q}\right) = \mathbf{Q}_{\mathrm{ext}}\left(\mathbf{q}, t\right) \tag{18}$$

3 Strategies of node selection and related quadrature

3.1 Description of the placement strategies

In the ANCF-C beam formulation, element nodes have traditionally been placed at the quadrature points used to evaluate the element matrices. For the strategy in [24], the element nodes are constrained to be coincide with the quadrature points, the number of element nodes are equal to that of quadrature points. When lower order shape functions are used, e.g. Lagrange polynomials, accurate integration can be obtained with the equal quadrature points. For higher order shape functions, e.g. Hermite interpolation polynomials, equal quadrature points are far from enough to give reasonable result. To break the constraints, a subset of the quadrature points for fully integration are used as the element nodes. The collocation nodes of the element can be decoupled from quadrature points that a strategy of node selection based on the complete quadrature set is required. As the quadrature rule is specified, the complete set of quadrature points and corresponding weights on the standard nondimensional domain $\xi \in [-1,1]$ are generated. A subset of these points is then selected as collocation nodes subject to endpoint retention, left–right symmetry, and node-count parity constraints. The unselected quadrature points are remained only to contribute to the numerical integration of the stiffness and mass matrices. The numbers of collocation nodes and quadrature points can thus be controlled independently, preserving their spatial relationship while avoiding the restriction on quadrature accuracy imposed by one-to-one identification.

This study examines this limitation and develops a compatible procedure for selecting nodes and performing numerical integration. Three strategies are constructed: equidistant nodes with closed Newton–Cotes quadrature, Legendre-type nodes with Legendre–Gauss–Lobatto quadrature, and Chebyshev-type nodes with Clenshaw–Curtis quadrature. These combinations are used to systematically investigate the influence of node placement on the accuracy, convergence, and computational efficiency of the ANCF-C beam element. The node placement strategy in [29] is compared with the proposed three strategies, which are denoted as equidistant (S1), Legendre-

type (S2), and Chebyshev-type (S3) placement. Fig.2 illustrates the distributions of node locations and quadrature points for five-node element and nine-node element-. Table 1 gives the formulations which are used to determine the interior quadrature-point positions for the three strategies. Where N_q denotes the number of quadrature points and k is the quadrature-point index.

For an element with n position nodes in the ANCF-C formulation, the n positional interpolation conditions are supplemented by two independent endpoint axial-gradient Hermite interpolation conditions. The scalar interpolation space therefore has dimension n+2. To obtain a full-rank discrete mass matrix, the complete quadrature set must contain at least $N_q \geqslant n$+2. In addition, the quadrature-point count must satisfy the structural requirements of the chosen integration rule. For a 5-node element, the minimum number of quadrature points is N_q =7. This value is admissible for S1 under the composite seven-point closed Newton–Cotes rule, for S2 under the Legendre–Gauss–Lobatto rule, and for S3 under the Clenshaw–Curtis rule. Accordingly, all three strategies use seven quadrature points. When n=9, the interpolation-space requirement becomes $N_q \geqslant 11$. S2 and S3 can both employ 11point quadrature rules, and therefore use N_q =11. By contrast, S1 uses the composite seven-point closed Newton–Cotes rule, for which the complete quadrature-point count must satisfy N_q =6k+1. The smallest admissible value is 13, which also meets the full-rank requirement. Thus, S1 uses N_q=13.

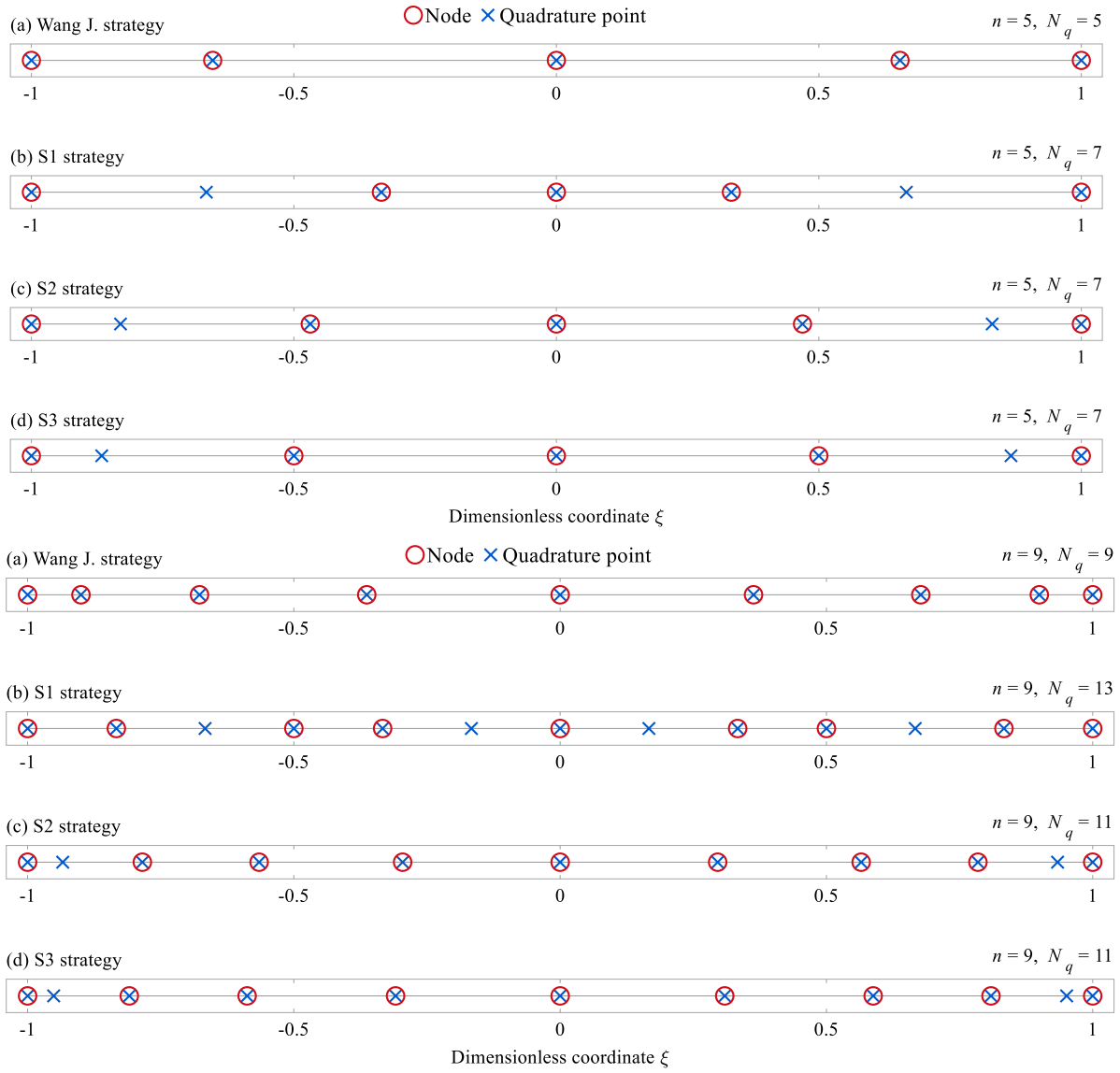


Fig2. Positions of nodes and quadrature points for five-node and nine-node elements

Table 1 Interior point distributions for the three strategies

Strategy	Node type	Quadrature rule	Interior quadrature points
S1	Equidistant nodes	Closed Newton–Cotes	$\xi_k = -1 + \frac{2(k-1)}{N_q - 1}$
S2	Roots of the derivative of a Legendre polynomial	Gauss–Lobatto	$P'_{N_q-1}(\xi) = 0$
S3	Roots of the derivative of a Chebyshev polynomial	Clenshaw–Curtis	$\xi_k^q = -\cos\left(\frac{(k-1)\pi}{N_q - 1}\right)$

3.2 Strategy of the node selection

The node selection procedure begins by prescribing the number of nodes n and generating the complete quadrature set, including both endpoints and its weights for the selected quadrature strategy. A total of n position points are then selected as collocation nodes under endpoint retention, left–right symmetry, and parity constraints. If the geometric constraints admit more than one candidate subset, a scaled Hermite interpolation matrix is constructed for each candidate. The candidates are screened using the matrix 2-norm condition number and a dimensionless basis-function amplification measure. The unselected quadrature points are not removed but remain fully involved in the evaluation of the mass and stiffness matrices.

The endpoints are retained so that the endpoint position vectors and material axial gradient vectors provide the Hermite boundary conditions and connect adjacent elements. Left–right symmetry is imposed to avoid an artificial bias toward either direction of the nondimensional coordinate. Node-count parity must also be satisfied. When the number of nodes n is odd, the number of quadrature points must be odd; the central point is retained, and other symmetric points are selected for exclusion. When the number of nodes n is even, only the central point is excluded if the number of quadrature points is odd, whereas one symmetric pair is selected for exclusion if the number of quadrature points is even. If multiple candidate subsets satisfy parity, endpoint retention, and left–right symmetry, all admissible symmetric subsets are enumerated. The 2-norm condition numbers of the scale-normalized Hermite interpolation matrices are compared first. Candidates with equal condition numbers are then compared using the dimensionless basis-function amplification measure, and the final configuration is selected by lexicographic minimization of these two quantities. The node selection procedure is summarized in Fig. 3.

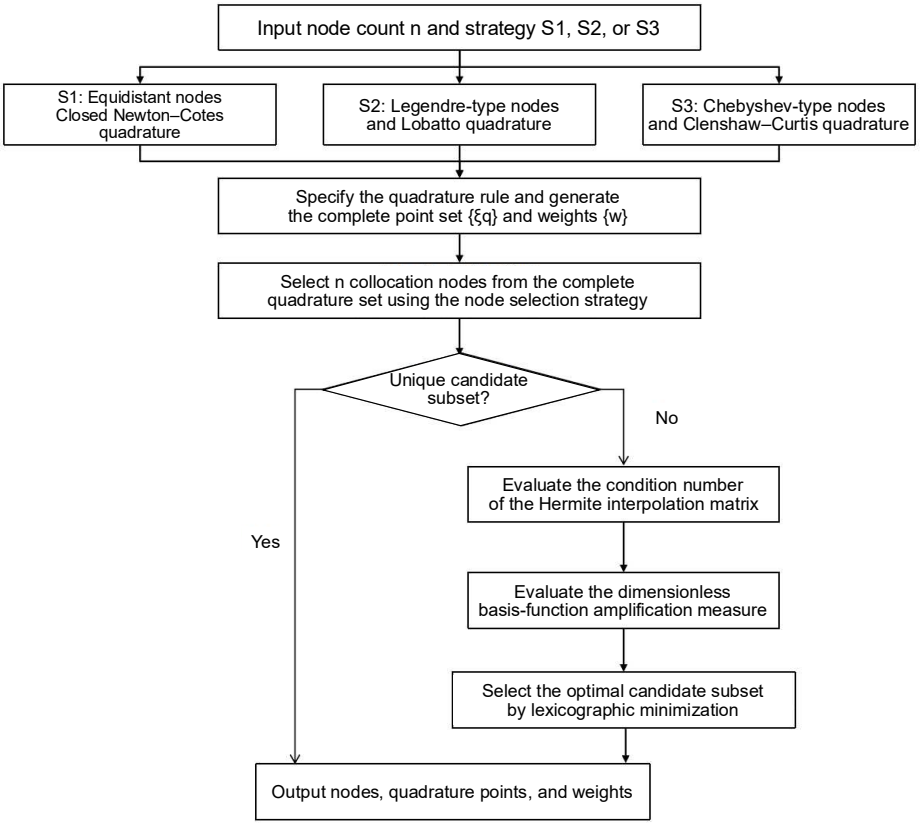


Fig.3 Procedure for selecting collocation-node positions

4 Numerical verification and discussion

In order to show the validity of the proposed ANCF elements and to illustrate the performance, several static and dynamic examples are considered.

4.1 Static examples

A uniform cantilever beam is subjected to a concentrated end moment M. Its geometric and material properties are illustrated in Fig.4. The applied moment is prescribed as $M = EI\theta / L$ and introduced in four loading increments. In this loading sequence, the beam is modeled using two five-node elements. The resulting deformed configurations at successive loading steps are shown in Fig.5. The beam curvature $\kappa = M / EI$ remains constant, and the final configuration forms a complete circle. The relevant parameters are listed in Table 2.

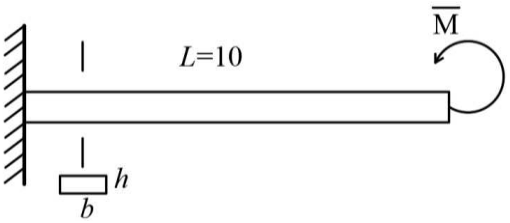


Fig.4 Pure bending of a uniform cantilever beam

Two complementary spatial refinement procedures are used for the static benchmark. The first holds the number of position nodes per element fixed while increasing the number of elements (mesh refinement). The second fixes the element count at one and increases the number of position nodes (high-order enrichment). The

first procedure thus assesses the effects of the placement strategies by varying the number of elements, whereas the second examines their influence on element performance by varying the number of position nodes.

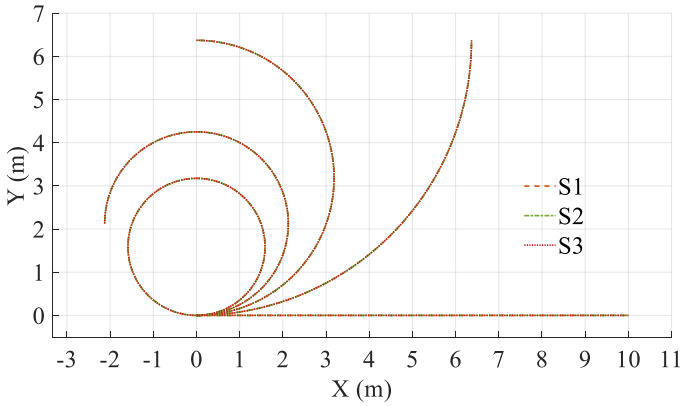


Fig.5 The deformed configurations of the cantilever beam

Table 2 Parameters of the bending benchmark

Parameter	Value	Unit
Beam length	10	m
Cross-sectional area	0.3	m^2
Second moment of area	0.00225	m^4
Young's modulus	20000	Pa

4.1.1 Comparison of the placement strategies

The cantilever is first analyzed using five-node ANCF-C elements, with the number of elements increased through 4, 8, 12, 16, 20, and 24 to investigate the influence of the placement strategy. The static equilibrium equations are solved by Newton–Raphson iteration. Fig.6 compares the absolute errors of the three strategies as the number of degrees of freedom increases. The absolute error is obtained by comparation of the analytical solution with respect to that obtained by proposed element.

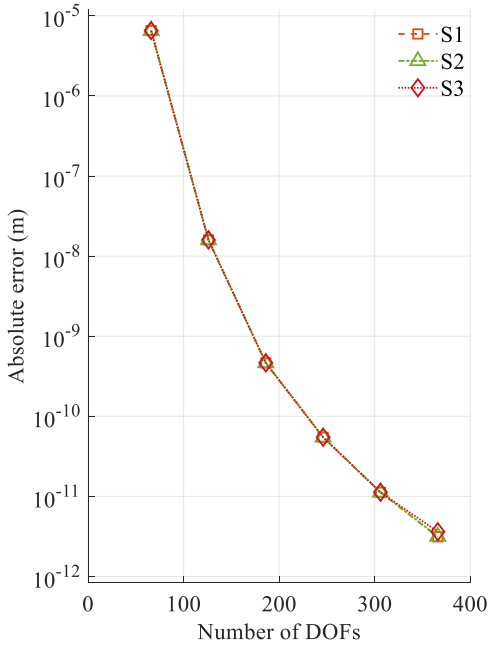


Fig.6 Absolute bending error versus the number of elements

S1, S2, and S3 have the same number of position nodes and the same total number of degrees of freedom.

Their differences can therefore be attributed primarily to the complete quadrature-point family, the collocation-node positions, and the corresponding quadrature weights. S2 exhibits a higher apparent convergence rate and the lowest absolute error in both the semicircular and full-circle bending tests. This indicates that, for the mesh range considered here, the Legendre–Gauss–Lobatto node placement combined with Lobatto quadrature is numerically better matched to the present Hermite-interpolated ANCF-C beam element. Computational efficiency is assessed through the relationship between solution time and accuracy, with emphasis on the time required to reach a given error level. As shown in Fig.7, within the grid discussed in this article, the element using S2 reaches the same accuracy in less time.

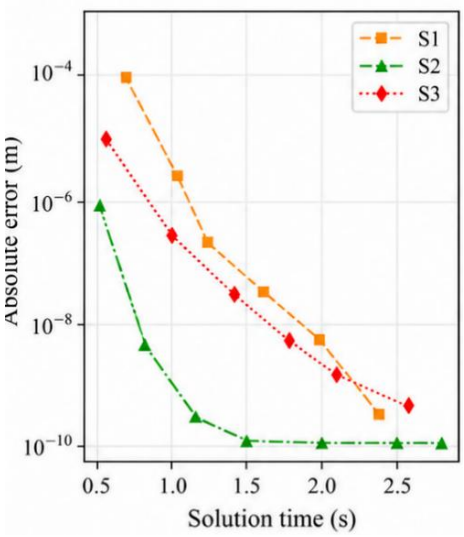


Fig.7 Absolute error versus solution time for the bending benchmark

4.1.2 Effects of node placement on element performance

To further examine the performance of the proposed ANCF-C element, bending tests are conducted using a single element with different numbers of nodes. Elements with 3、5、7 and 9-14 nodes are considered. All cases reproduce the corresponding bending configurations shown inFig.5. Fig.8 presents the absolute error of the single-element model as the number of nodes increases. Additionally, the proposed method is compared with that of Li and Zhong (2022) under identical operating conditions to evaluate its numerical accuracy and performance. The results demonstrate that the proposed method achieves higher accuracy under identical mesh discretization and loading conditions.

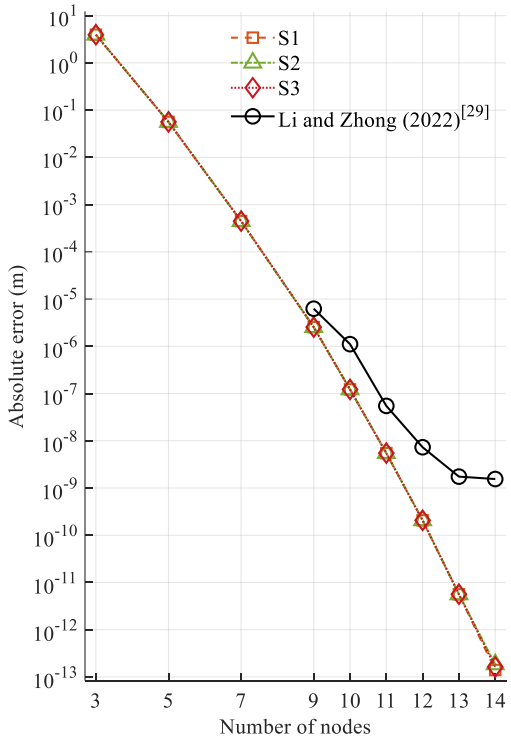


Fig.8 Absolute error versus number of the nember of nodes

4.2 Dynamic examples

The dynamic benchmark is a flexible cantilever released from an initially horizontal configuration under its own weight. The left end is fixed and the right end is free. The physical parameters are listed in Table 3and follow the flexible-pendulum benchmark associated with Omar and Shabana[6].

Table 3 Parameters of the freely falling flexible pendulum

Parameter	Value	Unit
Length	1.2	m
Young's modulus	0.7×10^6	Pa
Mass density	5540	kg/m³
Cross-sectional area	0.0016	m²
Second moment of area	8.533×10^{-6}	m⁴
Gravitational acceleration	9.81	m/s²

4.2.1 Comparison of the placement strategies

In the first dynamic test, the beam is discretized with two five-node ANCF-C elements and integrated to 1.1 s for g = 9.81 m/s². The results agree with those of Omar and Shabana[6]. Fig.9 Vertical displacement of the free end of the flexible pendulum shows the vertical displacement of the free end under a gravitational acceleration of 9.81 m/s². The responses of the present and reference models are in close agreement, and the three placement strategies produce very similar results. These results indicate that a converged solution can be obtained with a small number of elements.

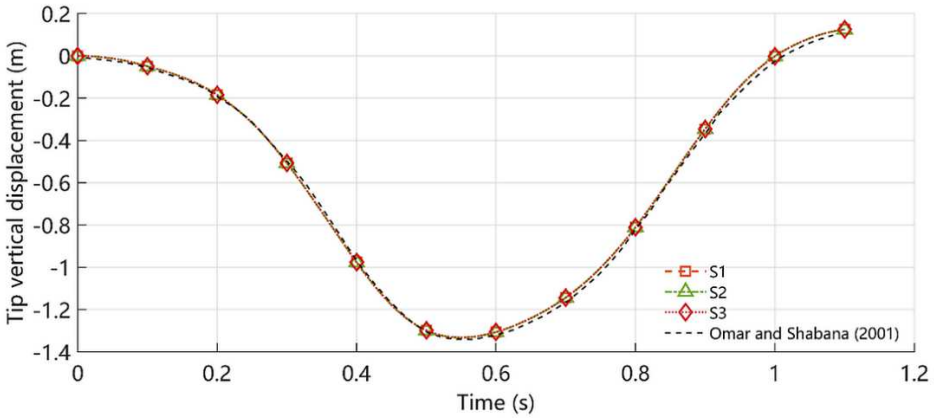


Fig.9 Vertical displacement of the free end of the flexible pendulum

For the standard benchmark with g = 9.81 m/s², the undamped system should conserve mechanical energy. Normalizing by a characteristic gravitational potential energy, the total mechanical energy drift is defined as

$$\delta_E(t) = \frac{\left|E_{\text{tot}}(t) - E_{\text{tot}}(0)\right|}{\rho A g L^2} \tag{19}$$

Fig.10 shows the continuous exchange among kinetic energy, strain energy, and gravitational potential energy during the downward and upward motion, while the total mechanical energy remains approximately constant.

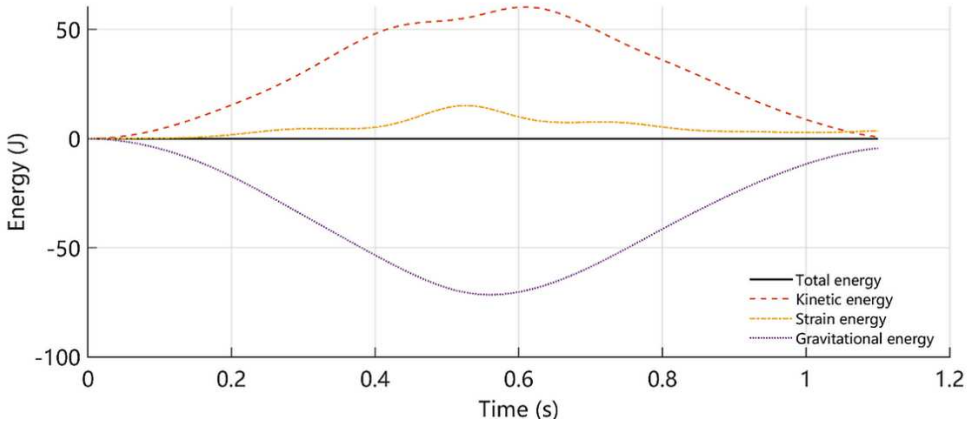


Fig10. Exchange among the mechanical energy components of the flexible pendulum

To further assess numerical stability and the ability of the proposed element to describe more pronounced overall motion and elastic deformation, the gravitational acceleration is increased to g = 50 m/s². two five-node elements are used, and all other parameters remain unchanged. The pendulum is released from its initial horizontal position at t = 0 s, and its configurations are recorded at successive times. The configurations obtained with the three strategies nearly coincide and are therefore represented by a single plot. Fig11 shows the time-dependent deformation during free fall. The results agree with those of Wang et al.[28], demonstrating the accuracy and robustness of the collocation-based element in large-deformation structural dynamics.

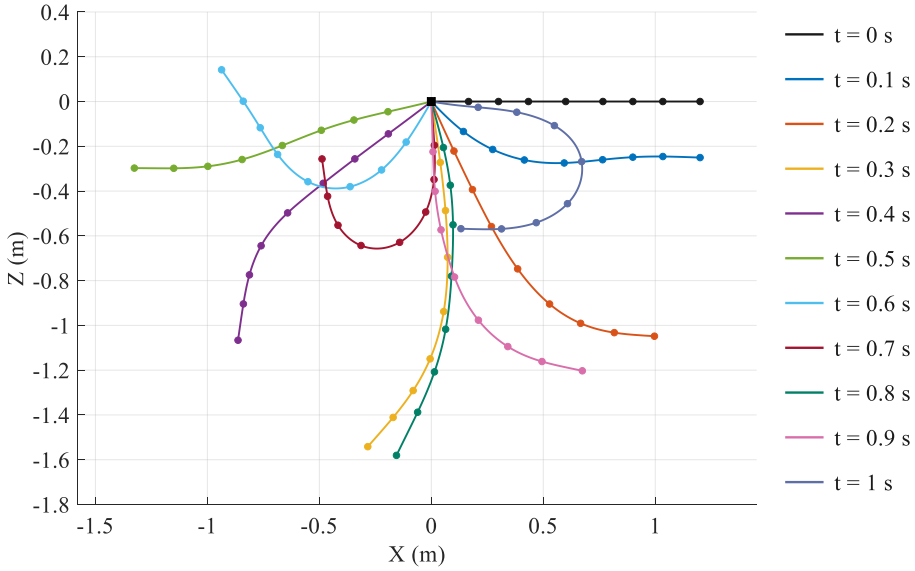


Fig.11 Free fall of the flexible pendulum

4.2.2 Effects of node placement on element performance

The influence of high-order interpolation on the transient solution is next considered with a single eight-node ANCF-C element. Under g = 9.81 m/s², Fig.12shows that the three computed free-end vertical-displacement histories remain close to each other and reproduce the main oscillation characteristics of the reference curve. This complements the two-element, five-node comparison in Fig.9 and indicates that a single enriched element can capture the global transient motion. Fig.13 shows the free-fall configurations obtained with a single nine-node ANCF-C element under g = 50 m/s². Fig.14 presents the time history of the absolute displacement error at the free end, defined as the absolute difference between the computed and theoretical vertical displacements. The free-end displacement error remains within 0.03 m.

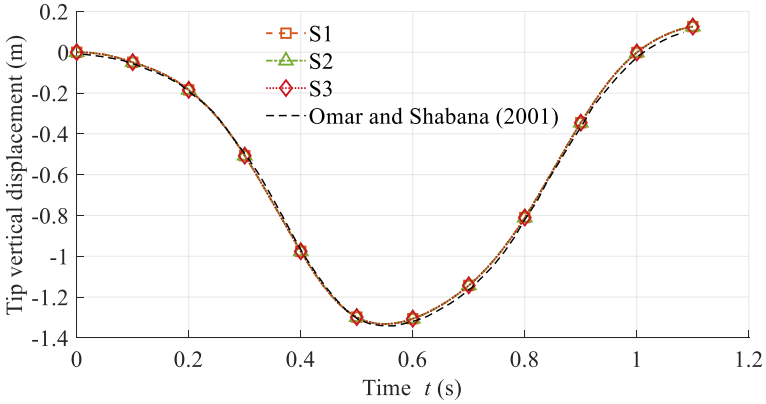


Fig.12 Vertical displacement of the free end of the flexible pendulum

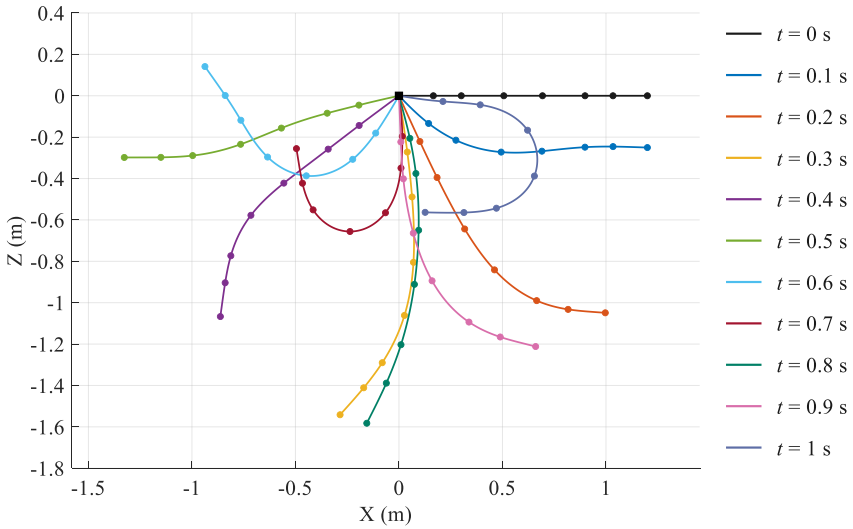


Fig.13 Free fall of the flexible pendulum

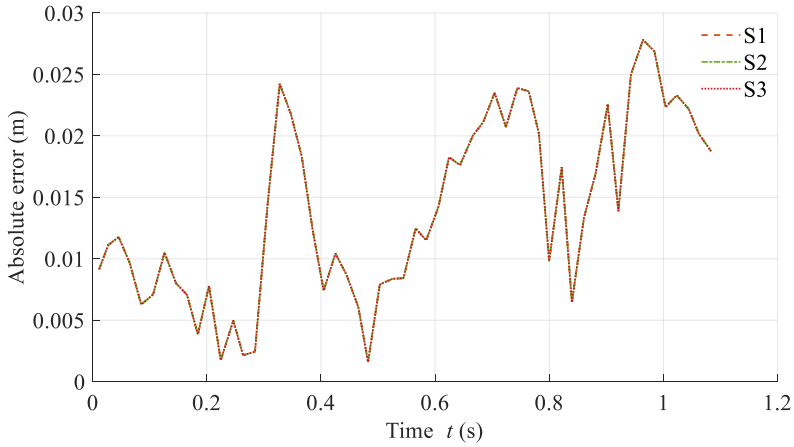


Fig.14 Displacement error at the free end of the pendulum

5 Conclusions

This study investigated the influence of node placement and numerical quadrature on the accuracy, convergence behavior, and computational efficiency of multi node ANCF-C beam elements. A quadrature-consistent node configuration framework was developed to coordinate spatial interpolation and numerical integration within the same element formulation. In this framework, position nodes are selected from a complete set of quadrature points, while the remaining quadrature points are retained for numerical integration. This allows the numbers of position nodes and quadrature points to be controlled independently without altering the underlying Hermite–Lagrange interpolation framework. Three configuration strategies were examined: uniformly distributed nodes combined with Newton–Cotes quadrature (S1), Legendre-based nodes combined with Legendre–Gauss–Lobatto quadrature (S2), and Chebyshev-based nodes combined with Clenshaw–Curtis quadrature (S3).

The static bending benchmarks demonstrated that node placement and quadrature selection have a significant influence on the numerical performance of the ANCF-C element. Two complementary refinement procedures were considered: increasing the number of elements while maintaining a fixed number of position nodes per element, and increasing the number of position nodes within a single element. For the semicircular and full-circle bending problems, spatial refinement generally reduced the absolute error in the free-end displacement. Among the three strategies, S2 exhibited the most favorable convergence behavior and generally produced the

lowest errors over the discretization examined. The comparison between computational cost and accuracy further indicated that S2 achieved a given accuracy with a shorter solution time in the reported bending tests. In addition, comparisons with the method of Li and Zhong (2022) showed improved accuracy for the proposed ANCF-C formulation under the investigated discretization and parameter settings. The dynamic benchmarks further examined the ability of the proposed formulation to describe large rotations and elastic deformations. Under standard gravitational acceleration, the predicted free-end displacement histories of the flexible pendulum reproduced the principal characteristics of the published reference response, with relatively small differences among the three node placement strategies. The corresponding energy histories showed continuous exchanges between kinetic, strain, and gravitational potential energies, while the total mechanical energy remained approximately constant. These observations support the consistency of the dynamic formulation for the standard-gravity benchmark.

References

[1] Shabana, A.A.: Definition of the slopes and the finite element absolute nodal coordinate formulation. Multibody System Dynamics 1(3), 339–348 (1997)

[2] Escalona, J.L., Hussien, H.A., Shabana, A.A.: Application of the absolute nodal co-ordinate formulation to multibody system dynamics. Journal of Sound and Vibration 214(5), 833–851 (1998)

[3] Berzeri, M., Shabana, A.A.: Development of simple models for the elastic forces in the absolute nodal co-ordinate formulation. Journal of Sound and Vibration 235(4), 539–565 (2000)

[4] Shabana, A.A., Yakoub, R.Y.: Three dimensional absolute nodal coordinate formulation for beam elements: theory. Journal of Mechanical Design 123(4), 606–613 (2001)

[5] Yakoub, R.Y., Shabana, A.A.: Three dimensional absolute nodal coordinate formulation for beam elements: implementation and applications. Journal of Mechanical Design 123(4), 614–621 (2001)

[6] Omar, M.A., Shabana, A.A.: A two-dimensional shear deformable beam for large rotation and deformation problems. Journal of Sound and Vibration 243(3), 565–576 (2001)

[7] Dufva, K.E., Sopanen, J.T., Mikkola, A.M.: A two-dimensional shear deformable beam element based on the absolute nodal coordinate formulation. Journal of Sound and Vibration 280(3–5), 719–738 (2005)

[8] Gerstmayr, J., Shabana, A.A.: Analysis of thin beams and cables using the absolute nodal co-ordinate formulation. Nonlinear Dynamics 45(1–2), 109–130 (2006)

[9] Gerstmayr, J., Irschik, H.: On the correct representation of bending and axial deformation in the absolute nodal coordinate formulation with an elastic line approach. Journal of Sound and Vibration 318(3), 461–487 (2008)

[10] Gerstmayr, J., Matikainen, M.K., Mikkola, A.M.: A geometrically exact beam element based on the absolute nodal coordinate formulation. Multibody System Dynamics 20(4), 359–384 (2008)

[11] Gerstmayr, J., Sugiyama, H., Mikkola, A.: Review on the absolute nodal coordinate formulation for large deformation analysis of multibody systems. Journal of Computational and Nonlinear Dynamics 8(3), 031016 (2013)

[12] Garcia-Vallejo, D., Mayo, J., Escalona, J.L., et al.: Efficient evaluation of the elastic forces and the Jacobian in the absolute nodal coordinate formulation. Nonlinear Dynamics 35(4), 313–329 (2004)

[13] Zhang, P., Duan, M., Gao, Q., et al.: Efficiency improvement on the ANCF cable element by using the dot product form of curvature. Applied Mathematical Modelling 102, 435–452 (2022)

[14] Taylor, M., Serban, R., Negrut, D.: An efficiency comparison of different ANCF implementations. International Journal of Non-Linear Mechanics 149, 104308 (2023)

[15] Taylor, M., Serban, R., Negrut, D.: Implementation implications on the performance of ANCF simulations. International Journal of Non-Linear Mechanics 149, 104328 (2023)

[16] Clenshaw, C.W., Curtis, A.R.: A method for numerical integration on an automatic computer. Numerische Mathematik 2(1), 197–205 (1960)

[17] Berrut, J.P., Trefethen, L.N.: Barycentric Lagrange interpolation. SIAM Review 46(3), 501–517 (2004)

[18] Trefethen, L.N.: Is Gauss quadrature better than Clenshaw–Curtis? SIAM Review 50(1), 67–87 (2008)

[19] Newmark, N.M.: A method of computation for structural dynamics. Journal of the Engineering Mechanics Division 85(3), 67–94 (1959)

[20] Shabana, A.A.: Dynamics of Multibody Systems. Cambridge University Press (2020)

[21] Lan, P., Tian, Q., Yu, Z.: A new absolute nodal coordinate formulation beam element with multilayer circular cross section. Acta Mechanica Sinica 36(1), 82–96 (2020)

[22] Zheng, Y., Shabana, A.A.: A two-dimensional shear deformable ANCF consistent rotation-based formulation beam element. Nonlinear Dynamics 87(2), 1031–1043 (2017)

[23] Shabana, A.A.: An overview of the ANCF approach, justifications for its use, implementation issues, and future research directions. Multibody System Dynamics 58, 433–477 (2023). https://doi.org/10.1007/s11044-023-09890-z

[24] Wang, J., Wang, T., Bian, H., Liu, W.: A novel collocation beam element based on absolute nodal coordinate formulation. Acta Mechanica 234, 2695–2707 (2023). https://doi.org/10.1007/s00707-023-03509-2

[25] Wang, J., Zhang, Y., Wang, T.: A planar beam element based on the absolute nodal coordinate formulation with a collocation-node strategy. Journal of Harbin Engineering University 46(7), 1405–1411 (2025) (in Chinese)

[26] Ishaquddin, M., Gopalakrishnan, S.: A novel weak form quadrature element for gradient elastic beam theories. Applied Mathematical Modelling 77, 1–16 (2020)

[27] Çevik, M., Savaşaneril, N.B., Sezer, M.: A review of polynomial matrix collocation methods in engineering and scientific applications. Archives of Computational Methods in Engineering 32, 3355–3373 (2025)

[28] Wang, C., Liu, J., Li, B., et al.: The absolute nodal coordinate formulation in the analysis of offshore floating operations, Part II: Code validation and case study. Ocean Engineering 281, 114650 (2023)

[29] Li H, Zhong H. Planar Weak Form Quadrature Beam Elements Based on Absolute Nodal Coordinate Formulation: A Structural Mechanics Approach[J]. Journal of Applied Mathematics and Physics, 2022, 10(11): 3475-3484.